Nonlinear Effects of SiO_2 Layers in Bulk Acoustic Wave Resonators

Carlos Collado, *Senior Member, IEEE,* Jordi Mateu, *Senior Member, IEEE,* David Garcia-Pastor, *Student Member, IEEE,* Rafael Perea-Robles, Alberto Hueltes, Susanne Kreuzer, and Robert Aigner.

***Abstract*— This work presents the development of a comprehensive distributed circuit model to account for the existing nonlinear effects in Bulk Acoustic Wave resonators (BAW). The comprehensiveness of the model and its distributed implementation allows for the inclusion of the nonlinear effects occurring in any layer of the BAW configuration, not only the piezoelectric layer. The model has been applied to evaluate the nonlinear contribution of the piezoelectric layer and silicon dioxide (SiO_2) layer in the Bragg reflector. The nonlinear manifestations are a function of the frequency of the driving fundamental tones. Accurate measurements of state of the art resonators validate the model proposed and confirm the contribution of the SiO_2 layer on the overall nonlinear performance.**

***Index Terms*—Nonlinearities, BAW, electro-acoustic, SiO_2, second harmonic, third harmonic, third order intermodulation product.**

I. Introduction

BULK acoustic wave (BAW) technology is becoming the main solution for the complex RF filtering of current and future mobile devices [1]. The increasing amount of services, frequency band and worldwide interoperability requirements for the handsets force the industry to place more and more high performance filters in a reduced space. Besides small footprint, power handling, high selectivity and low insertion losses, nonlinearities in BAW resonators have become a hot issue in the last years as the regulations and standards demand higher linearity.

Electro-acoustic dynamics of BAW resonators are intrinsically nonlinear. Nonlinear relations can be stablished between field magnitudes and it is not trivial to unambiguously identify what are the most important contributions to observable effects [2].

A circuital model is critical to understand the origin of nonlinearities. The model must be able to relate nonlinear properties of material that are independent of geometry, with experimental observations. After the first nonlinear distributed equivalent circuit of acoustic devices published in 1993 [3], extensive work has been done in the last 10 years. Reference [4] published a nonlinear distributed model for BAW resonators, which was based in the KLM circuit. This model was a phenomenological approach to describe the second harmonic (H2) generation and was surpassed by the non-lineal distributed Mason model [5], [6], which was based in the constitutive nonlinear equations. This later model was completed in [7] adding the thermal domain to the constitutive equations.

Authors of [2], [4]-[7] outlined the importance of measuring harmonics and intermodulation generation sweeping the frequency of the fundamental/s signal/s. The frequency pattern of a given observable must be consistent with the distributed model and it constitutes a fingerprint of the origin of the nonlinearity. In addition, different manifestations of nonlinearity, through different experiments, must be also consistent and explained with a unique model.

Those works, [4] and [7] using Solidly Mounted Resonators (SMR) and [2], [5], [6] using Thin-Film Bulk Acoustic Wave Resonators (FBAR), concluded that H2 and third order intermodulation (IMD3) was generated in the piezoelectric layer. Accordingly, all models developed were focused on the nonlinearities in the piezo-layer and none of them included the effects other layers could have in the nonlinearities. Specifically, the silicon dioxide (SiO_2) layers usually present in the Bragg Reflector of SMR resonators can play a significant role depending of the stack configuration.

This work experimentally validates the latter statement by performing three different experiments: a) generation of 2nd order harmonics H2 and 3rd order harmonics H3, b) third-order intermodulation products IMD3 and c) detuning with a DC voltage bias applied to the electrodes.

II. Constitutive Equations

A. Piezoelectric layers

The constitutive nonlinear electroacoustic equations for the piezoelectric layer are extensively explained in [5]-[7]. Those equations relate the field magnitudes stress *T*, strain *S*, electric field *E* and electric displacement *D* to each other using the

Manuscript received March, 2017. This work was supported in part by the Catalan Government through grant 2014 SGR 1103.
C. Collado, J. Mateu, D. García-Pastor, R. Perea-Robles and A. Hueltes are with the Signal Theory and Communications Dept. from Universitat Politècnica de Catalunya (UPC), Barcelona 08034, Spain (e-mail: collado@tsc.upc.edu). J.Mateu is also with Centre Tecnologic de Telecomunicacions de Catalunya (CTTC), PMT, Castelldefels, 08060, Spain.
S. Kreuzer and R. Aigner are with Qorvo, Inc., Orlando, FL.

constants c^E, e and ε^S, stiffness, piezoelectric and dielectric constant respectively. The equations according to the nomenclature described in [6] are:

$$T = c^E S - eE + \Delta T, \qquad D = eS + \varepsilon^S E + \Delta D, \tag{1}$$

where the nonlinear terms ΔT and ΔD are

$$\Delta T = c_2^E \frac{S^2}{2} + c_3^E \frac{S^3}{6} - \varphi_3 \frac{E^2}{2} + \varphi_5 SE, \qquad \Delta D = \varepsilon_2^S \frac{E^2}{2} + \varepsilon_3^S \frac{E^3}{6} - \varphi_5 \frac{S^2}{2} + \varphi_3 SE, \tag{2}$$

which depend on several 2nd order ($c_2^E, \varphi_3, \varphi_5, \varepsilon_2^S$) and 3rd order ($c_3^E, \varepsilon_3^S$) derivative constants. Using (1),(2) we can define the nonlinear constants as

$$c_{NL}^E = c^E \cdot \left(1 + \frac{c_2^E}{2c^E} S + \frac{c_3^E}{6c^E} S^2 + \frac{\varphi_5}{2c^E} E\right), \quad e_{NL} = e \cdot \left(1 - \frac{\varphi_5}{2e} S + \frac{\varphi_3}{2e} E\right), \quad \varepsilon_{NL}^S = \varepsilon^S \cdot \left(1 + \frac{\varepsilon_2^S}{2\varepsilon^S} E + \frac{\varepsilon_3^S}{6\varepsilon^S} E^2 + \frac{\varphi_3}{2\varepsilon^S} S\right), \tag{3}$$

in order to help a better understanding of the role of each parameter.

The model will be finally implemented using the strain S and the electrical displacement D as independent variables, and adding the nonlinear voltage sources T_c and V_c to a conventional distributed Mason model [5], [6]. As done in [2], [7], the piezoelectric layer is discretized into many unit cells of small thickness Δz, where the strength of the electric field is constant.

$$T = c^D S - \frac{e}{\varepsilon^S} D + T_C, \qquad E = \frac{D - eS}{\varepsilon^S} - V_C, \tag{4}$$

where

$$T_C = \Delta T + \frac{e}{\varepsilon^S} \Delta D, \qquad V_C = \frac{\Delta D}{\varepsilon^S} \Delta z \tag{5}$$

and the stiffened elasticity is defined as

$$c^D = c^E + \frac{e^2}{\varepsilon^S}. \tag{6}$$

B. Non-piezoelectric layers

For the non-piezoelectric layers, the nonlinear relation between stress and strain, truncated up to a third order, can be written as

$$T = c_{NP} S + T_C, \qquad T_C = \frac{1}{2} c_{2,NP} S^2 + \frac{1}{6} c_{3,NP} S^3, \tag{7}$$

in which the subscript NP indicates the material and $c_{2,NP}, c_{3,NP}$ are the nonlinear derivatives of the elastic constant $c_{NP,NL}$:

$$c_{NP,NL} = c_{NP} \cdot \left(1 + \frac{c_{2,NP}}{2c_{NP}} S + \frac{c_{3,NP}}{6c_{NP}} S^2\right). \tag{8}$$

III. Nonlinear model

A. Piezoelectric

The circuit model of the piezoelectric layer is the same than the one used in [2], [5]-[7]. Equations (4), (5) are implemented using the distributed Mason model, in which the equivalences *Force=Voltage*, *Particle velocity=Current* allow for an equivalent circuit implementation. This model discretizes the piezoelectric layer into many unit cells (slabs of thickness Δz), which account for electro-acoustic interactions (4) and the acoustic wave propagation in the thickness direction. Each cell obeys the telegrapher equations for an acoustic transmission line with distributed parameters [8]

$$C_{\Delta z} = \frac{\Delta z}{A c^D}, \qquad L_{\Delta z} = \Delta z \rho A, \qquad G_{\Delta z} = \frac{\Delta z}{A \eta^D}, \tag{9}$$

in which A, c^D, ρ, η^D are the resonators' area, stiffened elasticity, mass density and viscosity respectively.

Fig. 1 shows the nonlinear unit cell [2], [7] of the circuit model. The number of unit cells that must be cascaded depends on the highest frequency of interest. In our case we will discretize the piezoelectric in 60 unit cells.

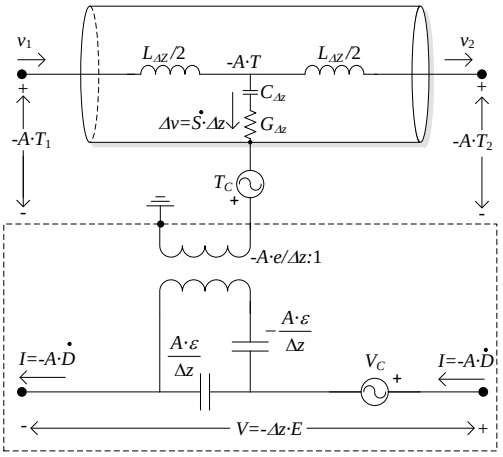

Fig. 1. Nonlinear unit cell of the piezoelectric layer [2], [7].

B. Non-piezoelectric

Two different approaches have been used to model a non-piezoelectric layer depending on the potential non-lineal behavior of the material.

1) Lineal layers

Acoustic wave propagation can be modeled with a conventional T-network circuit (Fig. 2a) for an acoustic transmission line with propagation constant γ and characteristic impedance Z_0:

$$\gamma = \alpha + j\frac{\omega}{v_A}; \quad Z_0 = \rho \cdot A \cdot v_A, \tag{10}$$

v_A being the phase velocity and α the attenuation constant [8]

$$\alpha = \frac{1}{2}\eta\omega^2\frac{\sqrt{\rho c}}{c^2}. \quad (11)$$

2) Discretized model for nonlinear layer

For the nonlinear case, the field magnitudes must be calculated at each point along the thickness of the layer. A discretized model [8] is again used (Fig 2b) with distributed inductance, capacitance and conductance according to (9) and nonlinear voltage sources T_c according to (7)

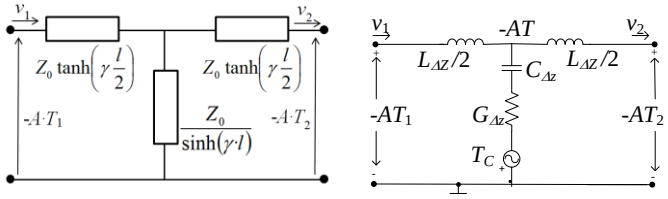

Fig. 2. Circuit models of the non-piezoelectric layers. T-network equivalent circuit of an acoustic transmission line (left) and nonlinear unit cell (right) of a discretized transmission line.

IV. Devices and Linear Measurements

Distributed nonlinear models can reproduce the standing-wave pattern of the fields along the thickness direction of the stack at a given frequency. The local nonlinear contribution to a given measurable magnitude, such as the second harmonic power at the electrodes of the resonator can be simulated. The frequency pattern of this measurable quantity is like a fingerprint of the origin of the nonlinearities, since each nonlinear constant will contribute in a different way as a function of frequency. This is because some of the constants, those appearing in ΔT and ΔD in (2), determine the sources T_c through (5), and those appearing in ΔD affect to V_c and T_c. Furthermore, as those constant are the results of derivatives with regard different independent magnitudes, S or E, the effect on the frequency pattern will be also different according to the different frequency pattern of S and E.

Fig. 3. Stack configuration of the measured SMR BAW resonator.

The main advantage of using distributed models is that it provides valuable information [2], [4]-[7] to characterize the materials and determine their nonlinear constants. In addition, a given set of nonlinear constant must be consistent with all the experimental results that those constants can determine.

In this article we discuss the experiments we have performed to unambiguously identify and quantify nonlinear constants in BAW resonators.

A. Description of the devices

The measured device is an Aluminum Nitride (AlN) based SMR resonator formed by more than ten layers. The thickness l of the AlN is 0.9 µm and the series resonance frequency is around 2.3 GHz. The layers of the electrodes and Brag reflector are plotted in Fig. 3. The stack used is similar to [9].

B. Linear fitting

A very good match between the linear measurements and the model is critical for an accurate model of the nonlinearities. Not only the main resonance must be accurately modeled, but also the out of band resonances appearing at higher frequency as we will discuss in next sections.

Fig. 4 shows the measured input impedance and the simulated response showing very good agreement.

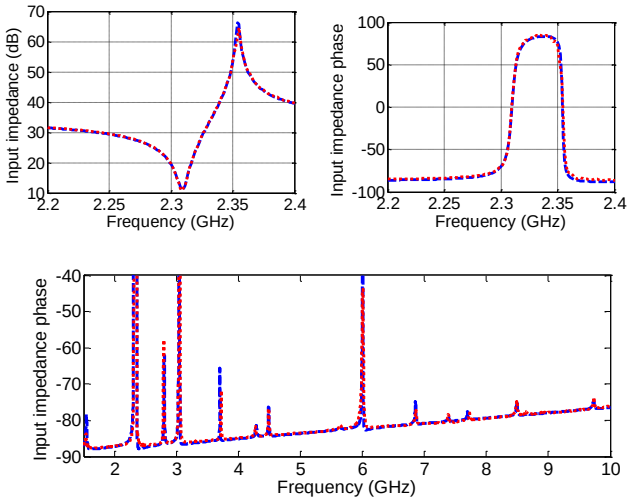

Fig. 4. Simulated (dashed blue) and measured (dotted red) narrowband (upper figures) and broadband (lower figure) input impedance of a BAW resonator.

V. Nonlinear Measurements

A main concern in BAW resonators is about the second order nonlinearities which are usually characterized by second harmonic H2 generation [2], [4]-[7], [10]

A. Narrowband Second Harmonic Measurements

Fig. 5 shows the measured second harmonic with a DUT input power of 21 dBm. As it was expected, there is a maximum at a frequency just above the series resonance of 2.32 GHz. At this frequency, the stress is maximum inside the piezoelectric layer [4] and there is consensus [2], [5]-[7] on the origin of the nonlinearity: the parameter φ_5, (δ_1 in [5], [6]) which sets the strain-dependent piezoelectric constant, or the electric field-dependent elasticity due to equivalent second-order interactions between physical domains. In fact, despite φ_5 having an effect on *Vc* and *Tc* according to (2)-(5), the main contributor to the H2 level at this frequency is the nonlinear source *Vc*.

Fig. 5 shows the second harmonic simulated with $\varphi_{5,AlN} = -17 \cdot e_{AlN}$. This value is exactly the same we obtained in [7]. The smooth ripple appearing is due to the

measurement system and its measured effect is included in the simulation [11]. The simulation matches the measured response related to the main resonance (peak at 2.34 GHz) but fails to model the additional peak appearing at 2.245 GHz. To understand where this peak is coming from, we have to take a look at the out of band resonances present in the broadband input impedance of the resonator. As it can be seen in Fig. 4, a small resonance shows at twice that frequency: 4.49 GHz. Apparently there is an acoustic mode at 4.49 GHz which is able to interact with H2 of the driving tone at 2.245 GHz, as the mode couples to the electrical domain the H2 measurement shows a high peak in Fig. 5. As the high frequency out of band resonances are strongly dependent on the stack configuration the linear response must be accurately modeled to reproduce this effect in simulations as introduced in previous Section IV. At a first glance, the term c_2^E of the piezoelectric constant can produce this high peak as shown in Fig. 5. The pair of values $c_{2,AlN}^E = -32.2 \cdot c_{AlN}^E$ and $\varphi_{5,AlN} = -23.8 \cdot e_{AlN}$ reproduces the measured frequency pattern.

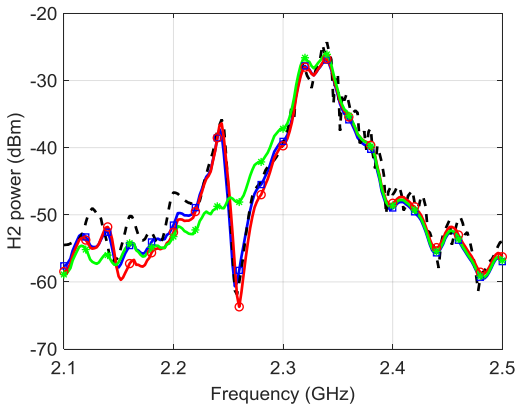

Fig. 5. Measured (dashed black) and simulated H2 for the cases: only $\varphi_{5,AlN}$ (green asterisks), $\varphi_{5,AlN}$ and $c_{2,AlN}^E$ (red circles), $\varphi_{5,AlN}$ and $c_{2,SiO}$ (blue squares).

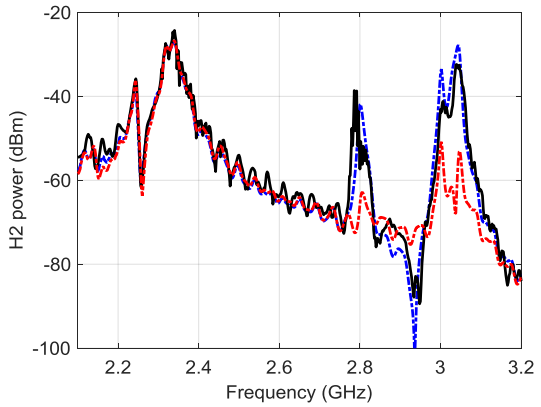

Fig. 6. Measured (solid black) and simulated broadband H2 for the cases: $\varphi_{5,AlN}$ and $c_{2,AlN}^E$ (dashed red), $\varphi_{5,AlN}$ and $c_{2,SiO}$ (dotted blue).

Nevertheless, the nonlinear term of the elastic constant c_2^E is not a uniquely able to produce this effect. A nonlinear elastic constant for the SiO_2 with $c_{2,SiO} = -6.4 \cdot c_{SiO}$ can produce the same effect as shown in Fig. 5. In the latter case, the nonlinearities of the AlN are set to $\varphi'_{5,AlN} = -18.7 \cdot e_{AlN}$ and $c_{2,AlN}^E = 0$. In this case, we have checked through simulations that the SiO_2 layer placed just underneath the bottom electrode is the predominant SiO_2 layer causing this H2 peak. This makes sense since the standing wave pattern of the strain in SiO_2 is dominated by the first layer at that frequency.

It is clear that additional measurements must be done to discern between those two working hypotheses: $(\varphi_{5,AlN}, c_{2,AlN}^E)$ and $(\varphi'_{5,AlN}, c_{2,SiO})$.

B. Broadband Second Harmonic Measurements

Broadband H2 measurements can help since the standing wave pattern at higher frequencies changes considerably within the stack. Fig. 6 shows the measured H2 from 2.1 GHz up to 3.2 GHz. As it can be seen, high H2 peaks appear at 2.8 GHz and 3 GHz. Note that the AlN nonlinear term $c_{2,AlN}^E$ cannot reproduce them, yet the SiO_2 term $c_{2,SiO}$ creates excellent agreement with measurements as can be seen in Fig. 6.

It is worth mentioning that in both scenarios we have introduced a nonlinear term for the AlN dielectric constant. The term $\varepsilon_2^S = 20 \cdot \varepsilon^S e_{AlN} / c_{AlN}^E$ must be taken in consideration to reproduce the out-of-resonance plateau of the H2 as shown in Fig. 7.

C. Narrowband IMD3 and H3

We have also performed IMD3 and H3 measurements. Two tones were applied with a tone spacing of $\Delta f = f_2 - f_1 = 1$ MHz and DUT input power of 30 dBm. Fig. 8 shows the measurements and simulations for the hypothesis $(\varphi_{5,AlN}, c_{2,AlN}^E)$. This hypothesis overestimates the IMD3 and H3 at resonance. Fig. 9 shows the measurements and simulations for the second hypothesis $(\varphi'_{5,AlN}, c_{2,SiO})$. This matches the measurements better. Note that no additional third order terms have been included. Therefore, third order intermodulation products and harmonics are coming from second order nonlinear terms by remix of the second order terms $(\varphi'_{5,AlN}, c_{2,SiO})$ with the fundamental signals.

Sticking to the confirmed 2nd hypothesis, we investigate which term is the main contributor to third order nonlinearities: $\varphi'_{5,AlN}$ or $c_{2,SiO}$. Fig. 10 shows simulations with $c_{2,SiO} = 0$ and Fig. 11 shows simulations with $\varphi_{5,AlN} = 0$. As it can be seen, $\varphi'_{5,AlN}$ slightly underestimates the IMD3 and fails to simulate the H3 below resonance. On the contrary $c_{2,SiO}$ overestimates the IMD3 and predict the H3 very well, which is completely dominated by this term.

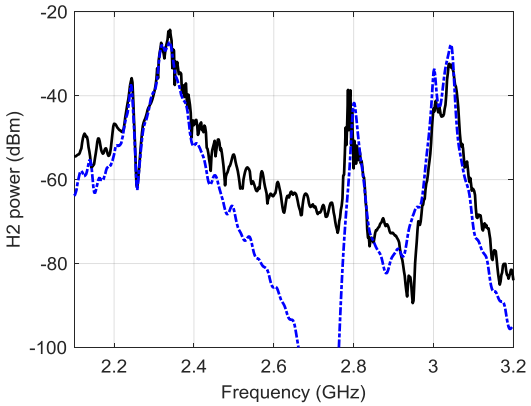

Fig. 7. Measured (solid black) and simulated broadband H2 for the cases $\varphi_{5,AlN}, c_{2,SiO}$ with $\varepsilon_2^S = 0$ (dotted blue).

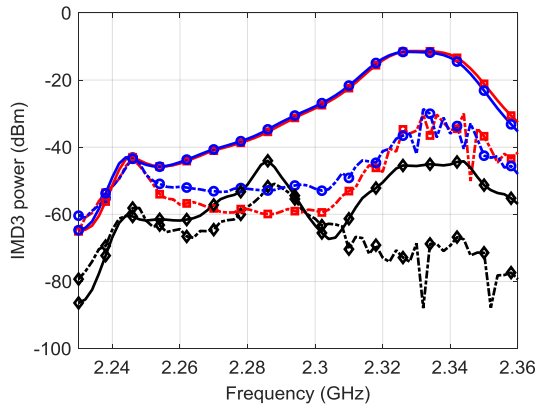

Fig. 8. Measured (dotted lines) and simulated (solid lines) IMD3 ($2f_1$- f_2 in blue circles and $2f_2$- f_1 red squares) and H3 ($3f_1$ in black diamonds) for the case $\varphi_{5,AlN}$ and $c_{2,AlN}^E$.

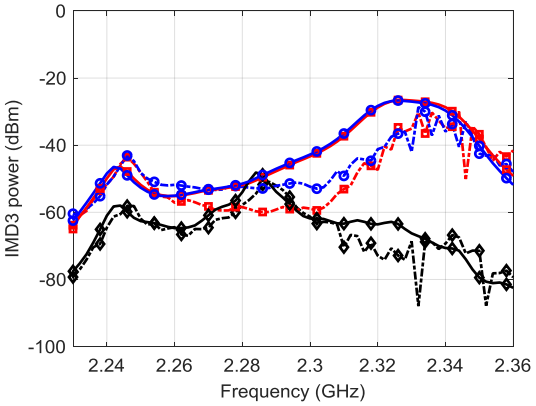

Fig. 9. Measured (dotted lines) and simulated (solid lines) IMD3 ($2f_1$- f_2 in blue circles and $2f_2$- f_1 red squares) and H3 ($3f_1$ in black diamonds) for the case $\varphi_{5,AlN}$ and $c_{2,SiO}$.

In our previous work on SMR BAW resonators [6], we stated that the IMD3 (with tone spacing big enough to avoid thermal effects) was due to $c_3{}^E$. H3 was not measured because the measurement bandwidth was limited to 50 MHz around resonance. Because the stack was different, we did not discover the contribution of the SiO_2 layers on the nonlinearities and we wrongly postulated that the IMD3 was directly generated by a third order nonlinear term $c_{3,AlN}^E = -111 \cdot c_{AlN}^E$. Here, we have performed simulations with this value and setting $c_{2,SiO} = 0$ and the IMD3 peak at resonance is exactly the same than the one resulting from $c_{2,SiO}^E$ as shown in Fig. 12. However, IMD3 and H3 out of resonance, between 2.23 GHz and 2.3 GHz, are not consistent as shown in Fig 12. It now seems clear than third order term $c_{3,AlN}^E$ is not the main contribution to the measured IMD3 for this stack.

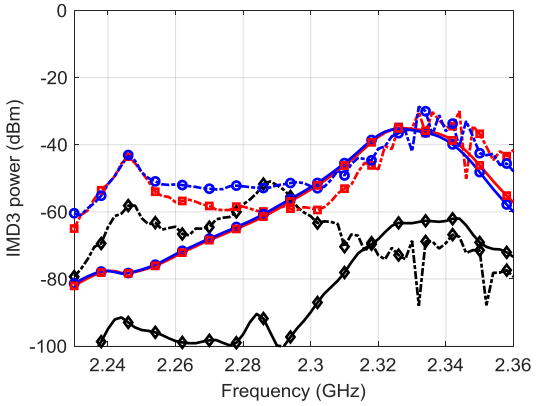

Fig. 10. Measured (dotted lines) and simulated (solid lines) IMD3 ($2f_1$- f_2 in blue circles and $2f_2$- f_1 red squares) and H3 ($3f_1$ in black diamonds) for the case only $\varphi_{5,AlN}$.

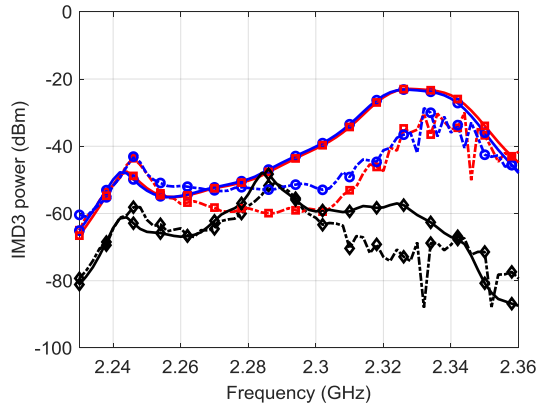

Fig. 11. Measured (dotted lines) and simulated (solid lines) IMD3 ($2f_1$- f_2 in blue circles and $2f_2$- f_1 red squares) and H3 ($3f_1$ in black diamonds) for the case only $c_{2,SiO}$.

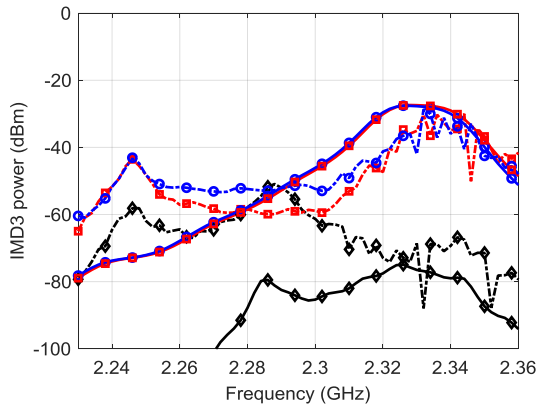

Fig. 12. Measured (dotted lines) and simulated (solid lines) IMD3 ($2f_1$- f_2 in blue circles and $2f_2$- f_1 red squares) and H3 ($3f_1$ in black diamonds) for the direct generation due to only $c_{3,AlN}^E$.

D. DC-Detuning

The third experiment is an S-parameters measurement while a DC bias voltage is applied at the electrodes. This must provide consistent results for the hypothesis to be confirmed. This experiment is of remarkable interest since the SiO_2 layers are not subject to the static electric field between electrodes, nor will static strain exist in the SiO_2 layers.

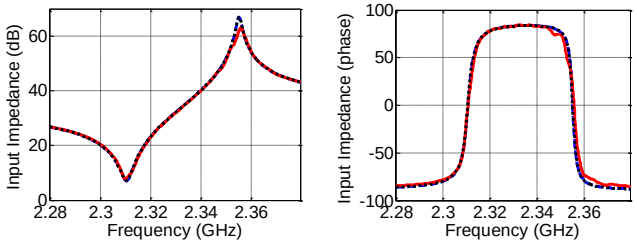

Fig. 13. Input impedance with +25 V of DC voltage, measured (solid red), HB simulation (dotted black) and close-form expression (dashed blue).

Although, the nonlinear model we are using is able to simulate the effects of a DC bias applied voltage, we have also derived new closed-form expressions, whose derivation is detailed in the Appendix. As a consequence, linear simulations may account for an applied DC voltage just by replacing the constants c_{AlN}^{E}, e_{AlN}, and ε^{S} by the terms

$$c_{AlN}^{E,DC} = c_{AlN}^{E} \cdot \left(1 - \frac{c_{2,AlN}^{E} e}{c_{AlN}^{E} c_{AlN}^{D} l} V_{DC} + \frac{1}{2} \frac{c_{3,AlN}^{E} e^{2}}{c_{AlN}^{E} \left(c_{AlN}^{D} l \cdot \right)^{2}} {V_{DC}}^{2} - \frac{\varphi_5}{l c_{AlN}^{E}} V_{DC} \right),$$

$$e_{AlN}^{DC} = e_{AlN} \cdot \left(1 + \frac{\varphi_5}{c_{AlN}^{E} l} V_{DC} \right), \qquad (12)$$

$$\varepsilon^{S,DC} = \varepsilon^{S} \cdot \left(1 - \frac{\varepsilon_2^{S}}{\varepsilon^{S} \cdot l} V_{DC} \right),$$

l being the piezoelectric thickness. In order to validate the close-form equations, Fig. 13 shows the measured and simulated input impedance for an applied voltage of +25 V. HB simulations using the nonlinear model and linear simulations using the constants described in (12) overlap perfectly.

Fig. 14 shows the frequency shifts of the series and shunt resonances in part-per-million for a voltage ranging from -25 V up to 25 V that was measured, and simulations using (12) for both hypotheses. The hypothesis $\left(\varphi_{5,AlN}, c_{2,AlN}^{E}\right)$ overestimates the frequency shift in comparison with measurements. On the other side, the results for the hypothesis $\left(\varphi'_{5,AlN}, c_{2,SiO}^{E}\right)$, where simulations and measurements match perfectly. This is the third and simplest independent experiment that confirms the hypothesis $\left(\varphi'_{5,AlN}, c_{2,SiO}^{E}\right)$. Using the provided formulation, it is a fast test to set the magnitude of $\varphi'_{5,AlN}$ and does require neither complex measurements nor nonlinear simulations. However, this experiment by itself does not give any information about the nonlinearities coming from the SiO_2 layers, which play a significant role in the generation of harmonics and intermodulation products as shown earlier.

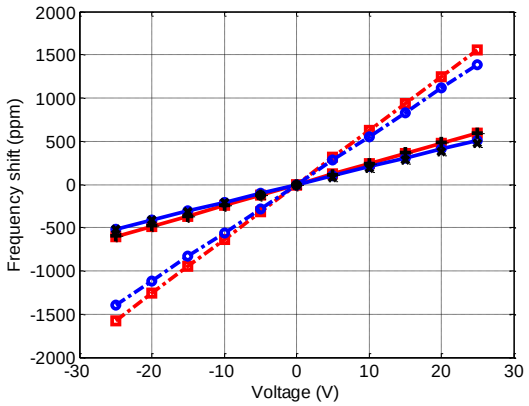

Fig. 14. Frequency shift of series (red squares) and shunt (blue circles) resonances in parts-per-millions of measured series resonance (black plus sign) and shunt resonance (black times sign), and simulations under $\left(\varphi_{5,AlN}, c_{2,AlN}^{E}\right)$ hypothesis (dashed lines) and $\left(\varphi'_{5,AlN}, c_{2,SiO}^{E}\right)$ hypothesis (solid lines).

VI. Nonlinearities in other layers

Other materials, such as the aluminum (Al) or the tungsten (W), could also contribute on the nonlinearities. In fact, both, Al and W, can reproduce the narrowband H2 behavior of Fig. 5 if appropriate $c_{2,Al}^{E}$ or $c_{2,W}^{E}$ terms are chosen. However, those hypotheses fail to model the broadband H2 response and they overestimate by far the IMD3.

It is also worth to mention that other third order nonlinear terms might also contribute to the direct IMD3 generation. This is for instance the case of the third order terms of elastic constant of the layers in the Bragg reflector, such as SiO_2 or W layers ($c_{3,SiO}^{E}$ and $c_{3,W}^{E}$ respectively), which could be considered to improve the match between simulations and measurements. Those terms, with the proper sign, might cancel out the IMD3 rising from remixing effects at frequencies around 2.32 GHz, and shift the simulated maximum IMD3 towards higher frequencies, giving a more accurate fitting to the measured IMD3. However, further experiments and research need to be done to properly discern and quantify the contribution of these layers SiO_2 and/or W.

VII. Conclusions

Unexpected second harmonic peaks may appear at some frequencies in BAW and FBAR resonators. When the device is driven at a frequency close to the resonance frequency, such that an out of band resonance exists at twice that frequency, the resonating conditions enhance the H2 and the output H2 power may become significant. For the particular stack studied in this paper we have unambiguously demonstrated that the silicon dioxide layer below the bottom electrode is responsible for this effect by three different experiments: broadband H2, IMD3 and H3, and DC detuning. Once, well stablished the origin of this anomalous effect, it may be corrected by modifying the design of the Bragg reflector and electrodes slightly to avoid out of band resonances close to twice the

main resonance.

For the resonator we have measured, the IMD3 and H3 were also dominated from the second order nonlinear silicon dioxide trough remixing effects.

The harmonic and intermodulation experiments were consistent with linear measurements of the input impedance of the resonator under a DC bias voltage. We also provide new closed-form expressions which agree perfectly with the nonlinear simulations.

APPENDIX I

Using (1) and (2), and considering negligible the term φ_3 according to the simulations of Section-V, we can write the nonlinear relation between stress, strain and electric field

$$T = \mathrm{c}^{\mathrm{E}} S - eE + \frac{1}{2} c_2^E S^2 + \frac{1}{6} c_3^E S^3 + \varphi_5 SE. \tag{13}$$

In order to characterize the DC feed contribution, the electric field and strain can be modelled as the sum of the contributions of the static magnitudes E_{DC} and S_{DC} produced by the DC voltage and the electric field and strain produced by the fundamental signal with peak amplitudes E_0 and S_0,

$$\begin{aligned} S &= S_{DC} + S_0 \cos(\omega t), \\ E &= E_{DC} + E_0 \cos(\omega t). \end{aligned} \tag{14}$$

By use of (13), and selecting the terms that affect the strain and electric field at the fundamental frequency, we can write

$$\begin{aligned} T = \Big(& c^E + c_2^E S_{DC} + \frac{1}{2} c_3^E {S_{DC}}^2 + \frac{1}{8} c_3^E {S_0}^2 \\ & + \varphi_5 E_{DC} \Big) S_0 \cos(\omega t) - (e - \varphi_5 S_{DC}) E_0 \cos(\omega t). \end{aligned} \tag{15}$$

The saturation term $\frac{1}{8} c_3^E {S_0}^2$ that does not depend on the DC bias voltage can be neglected for low power levels, and (15) can be written as

$$T = c^{E,DC} S_0 \cos(\omega t) - e^{DC} E_0 \cos(\omega t), \tag{16}$$

where the stiffness and piezoelectric constants modified by the DC voltage are respectively

$$\begin{aligned} c^{E,DC} &= c^E \cdot \left(1 + \frac{c_2^E}{c^E} S_{DC} + \frac{1}{2} \frac{c_3^E}{c^E} {S_{DC}}^2 + \frac{\varphi_5}{c^E} E_{DC} \right), \\ e^{DC} &= e \cdot \left(1 - \frac{\varphi_5}{e} S_{DC} \right). \end{aligned} \tag{17}$$

The strain produced by the DC voltage is

$$S_{DC} = \frac{e}{c^E} E_{DC} = \frac{e}{c^E} \left(\frac{-V_{DC}}{l} \right), \tag{18}$$

l being the thickness of the piezoelectric layer. Therefore, we can define and effective elastic $c^{E,DC}$ and piezoelectric e^{DC} constants under DC bias voltage as

$$\begin{aligned} c^{E,DC} &= c^E \cdot \left(1 - \frac{c_2^E e}{(c^E)^2 l} V_{DC} + \frac{1}{2} \frac{c_3^E e^2}{(c^E)^3 l^2} {V_{DC}}^2 - \frac{\varphi_5}{c^E l} V_{DC} \right), \\ e^{DC} &= e \cdot \left(1 + \frac{\varphi_5}{c^E l} V_{DC} \right). \end{aligned} \tag{19}$$

The contribution of the nonlinear term ε_2^S can be taking into account straightforward just replacing

$$\varepsilon^{S,DC} = \varepsilon^S \cdot \left(1 - \frac{\varepsilon_2^S}{\varepsilon^S \cdot l} V_{DC} \right). \tag{20}$$

The modified terms of (19) and (20) can be used instead of c^E, e and ε^S in linear simulations.

REFERENCES

[1] A. Tag and C. Ruppel, "RF Acoustic for Mobile Communication: Challenges and Modern Solutions", *IEEE Microwave Magazine*, vol. 16, no. 7, pp. 22-24, Jul. 2015.

[2] D. A. Feld, D. S. Shim, S. Fouladi, and F. Bayatpur, "Advances in nonlinear measurement & modeling of bulk acoustic wave resonators" *2014 IEEE International Ultrasonics Symposium*, Chicago, IL, 2014, pp. 264-272.

[3] Y. Cho and J. Wakita, "Nonlinear equivalent circuits of acoustic devices,", *1993 IEEE Ultrasonics Symposium*, Baltimore, MD, 1993, pp. 867-872 vol.2.

[4] C. Collado, E. Rocas, J. Mateu, A. Padilla, and J. M. O'Callaghan, "Nonlinear Distributed Model for Bulk Acoustic Wave Resonators", *IEEE Transactions on Microwave Theory and Techniques*, vol. 57, no. 12, pp. 3019-3029, Dec. 2009

[5] D. S. Shim and D. A. Feld, "A general nonlinear Mason model of arbitrary nonlinearities in a piezoelectric film", *2010 IEEE International Ultrasonics Symposium*, San Diego, CA, 2010, pp. 295-300.

[6] D. S. Shim and D. A. Feld, "A General Nonlinear Mason Model and Its Application to Piezoelectric Resonators", *International Journal of RF and Microwave Computer-Aided Engineering*, vol. 21, no. 5, Sep. 2011

[7] E. Rocas, C. Collado, J. Mateu, N. D. Orloff, J. C. Booth and R. Aigner, "Electro-thermo-mechanical model for bulk acoustic wave resonators", *IEEE Transactions on Ultrasonics, Ferroelectrics, and Frequency Control*, vol. 60, no. 11, pp. 2389-2403, Nov. 2013.

[8] B. A. Auld, *Acoustic Fields and Waves in Solids*, vol. 1, Malabar, FL: Krieger, 1990.

[9] A. Tajic et al., "No-drift™ BAW-SMR: Over-moded reflector for temperature compensation", *2016 IEEE International Ultrasonics Symposium*, Tours, 2016, pp. 1-4.

[10] E. Rocas, C. Collado, J. C. Booth, E. Iborra, and R. Aigner, "Unified model for Bulk Acoustic Wave resonators' nonlinear effects," *2009 IEEE International Ultrasonics Symposium*, Rome, 2009, pp. 880-884.

[11] C. Collado et al., "First-Order Elastic Nonlinearities of Bulk Acoustic Wave Resonators", *IEEE Transactions on Microwave Theory and Techniques*, vol. 59, no. 5, pp. 1206-1213, May 2011.